Al-Mustansiriyah Journal of Science
ISSN: 1814-635X (print), ISSN:2521-3520 (online) Volume 32, Issue 4, 2021 DOI: http://doi.org/10.23851/mjs.v32i4.1039

Research Article **Open Access**

Thermal Effect in a 3-D Simulation within Multilayer Thin Film of Ultrafast-Pulsed Laser

Muhaiman A. Abdul-Hussain*, Haidar J. Mohamad

Department of Physics, College of science, Mustansiriyah University, Baghdad, IRAQ.

*Correspondent contact: muhaimanali@uomustansiriyah.edu.iq

Article Info

Received
05/07/2021

Accepted
01/08/2021

Published
20/11/2021

ABSTRACT

Hard disk drive (HDD) and storage media have the potential to revolutionize future information technology. Heat-assisted magnetic recording (HAMR) is a promising method for increasing hard disk storage density and it is one of the applications of this study. The essential component of nanoscale spintronic devices is spin current. The simulation of a thermal gradient to generate a pure spin current using an ultrafast femtosecond (fs) laser in a multilayer thin film is presented. The trilayer sample (ferromagnetic/spacer/magnetic insulator) is the candidate to achieve the spin current. Ultrafast laser with fs pulse width simulated to creates a spin diffusion spark. These pulses penetrate within the trilayer reaching the magnetic insulator due to the penetration depth that record the effect. COMSOL Multiphysics software® is used to simulate the thermal behavior within the trilayer with three-dimensional (3-D) view. The thickness of the ferromagnetic layer (Ni81Fe19) has been shown to generate a high-temperature gradient within the magnetic insulator and therefore a larger spin current.

KEYWORDS: Spintronics; Spin current; Ultrafast laser; HAMR; Ferromagnetic materials; Spin current generation; COMSOL Multiphysics

الخلاصة

القرص الصلب ووسائط التخزين لديها القدرة على إحداث ثورة في تكنولوجيا المعلومات في المستقبل. يعد التسجيل المغناطيسي بمساعدة الحرارة (HAMR) طريقة واعدة لزيادة سعة التخزين على القرص الصلب وهو أحد تطبيقات هذه الدراسة. المكون الأساسي لأجهزة spintronic النانوية هو تيار برم الإلكترون. يتم عرض محاكاة التدرج الحراري لتوليد تيار دوران نقي باستخدام ليزر فيمتو ثانية فائق السرعة في فيلم رقيق متعدد الطبقات. العينة ثلاثية الطبقات (مادة فيرومغناطيسية/ فاصل/عازل مغناطيسي) سوف تستخدم للحصول على تيار برم الإلكترون. ليزر فائق السرعة بعرض نبضة فيمتو ثانية يتم محاكاته لبدء الحصول على انتشار برم الإلكترون. تخترق هذه النبضات إلى داخل الطبقة الثلاثية لتصل إلى العازل المغناطيسي بسبب عمق الاختراق الذي يسجل برم الإلكترون. تم استخدام برنامج COMSOL Multiphysics® لمحاكاة السلوك الحراري داخل الطبقة الثلاثية مع عرض ثلاثي الأبعاد. لقد ثبت أن سمك الطبقة الفيرومغناطيسية ($Ni_{81}Fe_{19}$) ضروري لتوليد تدرج حراري عالي داخل العازل المغناطيسي وبالتالي تيار دوران أكبر

INTRODUCTION

Pure spin currents are made up of a flow of spins with no net charge present. There are no losses associated with electrical resistance when such pure spin currents are created with no associated charge currents, making it possible to develop a new generation of low power and environmentally friendly devices utilizing the spin of the electron, known as Spintronics [1-3]. Spin currents are important in spintronics, much as charge currents are in electronics. The spin current carries an angular momentum that can be passed to a ferromagnetic (FM) layer, causing magnetization oscillations or even entirely flipping it. This phenomenon is called spin transfer torque (STT) [4, 5]. In the last few years, several authors have reported the generation and measurement of spin current using the spin Hall effect [SHE] [6-9] as well as a thermal gradient using the spin Seebeck effect [SSE] [10-12]. Because of its potential for increased storage area density, heat-assisted magnetic recording (HAMR) has been suggested for the next generation of hard disk drive [13]. Shingled magnetic recording (SMR) [14], bit-patterned media (BPM) [15] and microwave-assisted magnetic recording (MAMR) [16] are other techniques that increase the density of hard disk storage. In HAMR systems, the laser is considered as a means to momentarily heat the medium, which makes it sensitive and more susceptible to magnetic effects and enables writing

to much smaller areas and far greater amounts of data on a disk [17].

Jian-Gang Zhu and Hai Li [18] presented a micromagnetic modeling study of heat-assisted magnetic recording methods by using the Landau-Lifshitz-Bloch equation [19]. Shaomin Xiong et al. suggested a magnetic recording-based technique for performing in situ protrusion measurements as well as assisting in the adjustment of the write spacing [20]. Another way to produce a spin current is to use an ultrafast fs laser in a multilayer thin film, where the ultrafast laser generates a spark of spin diffusion to obtain the spin current. In a previous study, H. J. Mohamad et al. [21], succeeded in generating spin current by ultrafast laser in a multilayer thin films experimentally, but they did not consider the effect of ferromagnetic layer thickness on spin current generation. This can be exploring in details and study the effect of the layer thickness.

In the present study, we simulated thermal behavior induced by ultrafast fs laser within the trilayer $Ni_{81}Fe_{19}$ (Py)/Cu/$Y_3Fe_5O_{12}$ (YIG) using COMSOL Multiphysics, which is a strong immersive simulation platform for solving and modeling a wide range of research and technical problems [22], where a 3-D model was designed. This sample chosen to be a suggestion in the recording media devices. The YIG plays a good candidate to generate a spin current due its properties. Therefore, the simulation considered each parameter carefully in the 3D model for instance the thermal boundary conditions and the effect between each layer. The sample size has the same size of the laser spot size, and the surface effect is canceled because it is out of this work and does not affect on the presented results. The results show good describing to the penetration depth as well as the temperature gradient.

Theoretical Consideration

Ultrafast lasers produce light pulses that are shorter than a few tens of picoseconds (ps), and therefore involve femtosecond (fs) and picosecond (ps) lasers [23, 24]. Ultrafast lasers provide new opportunities in a vast scope of micro and nanotechnology applications and users, including mechanics, electronics, biology and medicine and in several others [25, 26]. Pulses of an ultrafast laser were submerged into the sample layers over a fs time scale. The fast increase in temperature inside the sample can thus be formulated using a 3-D heat diffusion equation [27]:

$$\frac{1}{D}\frac{\partial T}{\partial t} = \frac{\partial^2 T}{\partial x^2} + \frac{\partial^2 T}{\partial y^2} + \frac{\partial^2 T}{\partial z^2} + \frac{g(x,y,z,t)}{k} \quad (1)$$

Where *g(x,y,z,t)* is the absorbed power density within the sample, is thermal diffusivity *D* could be represented by *(D = k /ρ Cp), k, ρ, Cp* are the thermal conductivity, the material density, and the heat capacity per unit mass, respectively.

The suggested structure (ferromagnetic/spacer/ magnetic insulator) considered generating the spin current within the magnetic insulator (YIG) layer using an ultrafast laser directed at the sample structure. The distribution of the electric field in the active layer(s) is used to calculate the absorbed power density (heat source) in the heat diffusion equation and the temperature in each layer of the stack. The model specifies the transmission/ reflection coefficients at the film interfaces by considering multiple transmission and reflection [28]. The high-power absorption induced by ultrafast laser occurs predominantly within the Py and Cu layers, due to the high extinction coefficient of Py and Cu layers. The other layers in the stack are either comprehensive or negligible value of the extinction coefficients. Consequently, only a two-layer absorption model as shown in Figure 1 is used here, with the outer layers assumed to be semi-infinite in extent. The Poynting vector links a complex wave's time-averaged power per unit area (W/m^2) to electric and magnetic fields:

$$\langle S_m \rangle = \frac{1}{2}\Re\{E_m \times H_m\} \quad (2)$$

Therefore, the power absorbed per unit volume in layer m is:

$$\Re\{-\nabla \cdot \langle S_m \rangle\} = k_0 c \varepsilon_0 n_m \kappa_m |E_m|^2 \quad (3)$$

where $|\boldsymbol{E}m|^2 = \boldsymbol{E}m.\boldsymbol{E}^*$ and the total electric field in each layer is given by:

$$E_m = T_m e^{jk_0(n_m + j\kappa_m)z} X + R_m e^{-jk_0(n_m + j\kappa_m)(z-d_m)} X$$

In each layer, the magnitude of the electric field is thus:

$$|E_m|^2 = |T_m|^2 e^{k_0 \kappa_m^2} + |R_m|^2 e^{k_0 \kappa_m (z-d_m)} + 2|T_m R_m| e^{-k_0 \kappa_m d_m} cos(k_0 n_m (2z - d_m) + \varphi_m) \quad (4)$$

where $\varphi_m = tan^{-1}\left(\frac{\Im\{T_m R_m\}}{\Re\{T_m R_m\}}\right)$

To facilitate correct scaling of the power density in the medium to the experimental laser power, the

power density in equation (3) is normalized to the incident power to compare the difference in the power curve clearly:

$$\Re\left\{-\nabla\cdot\frac{\langle S_m\rangle}{\langle S_i\rangle}\right\} \quad (5)$$

where $\langle Si\rangle$ is the time-averaged power density of the incident electric field. The normalized power density can then be written as:

$$\Re\left\{-\nabla\cdot\frac{\langle S_m\rangle}{\langle S_i\rangle}\right\}=2k_0\frac{n_m k_m}{n_i}\frac{|E_m|^2}{I_i^2} \quad (6)$$

where n_m and n_i are the refractive indices of the transmitted and incident media, respectively, and k_m is the refractive index's imaginary part. $\boldsymbol{E}_m$ is the transmitted electric field in layer m, I_i is the incident electric field magnitude that takes the form $I_i^2=\tau_{12}^2E_1^2$ for the first layer, where $\tau_{12}=2\,n_1/(n_1+n_2)$, where n_1 and n_2 are the refractive indices of the incident and transmitted media. For the air/Al_2O_3 interface, n_1 and n_2 represent the refractive index of air and the Al_2O_3 layer, respectively.

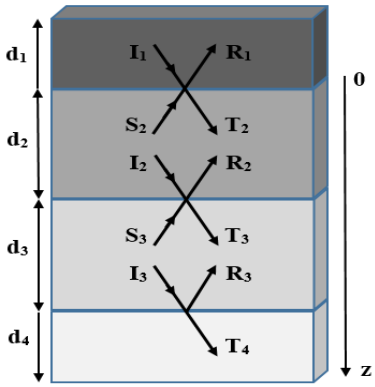

Figure 1. The transmission/reflection model within multilayer concept. *I*, *R* and *T* are the incident, reflected and transmitted field amplitudes respectively, while *S* is the amplitude of the field reflected from the next interface, *d* is the layer thickness.

MATERIALS AND METHODS

The present work illustrates a 3-D simulation of the thermal effect within a multilayer thin film as a result of ultrafast laser optical excitation using COMSOL Multiphysics version 5.5 software®. A 3-D model was created using a Heat Transfer in Solids (ht) interface with a time-based study as shown in Figure 2.

The sample is designed as a multilayer 3-D cube with width and depth of (3 nm) and height (2 nm) for the Al_2O_3, Cu (8 nm), Py (8 nm), YIG (58 nm), and $Gd_3Ga_5O_{12}$ (GGG) (0.9325 µm), as shown in Figure 3.

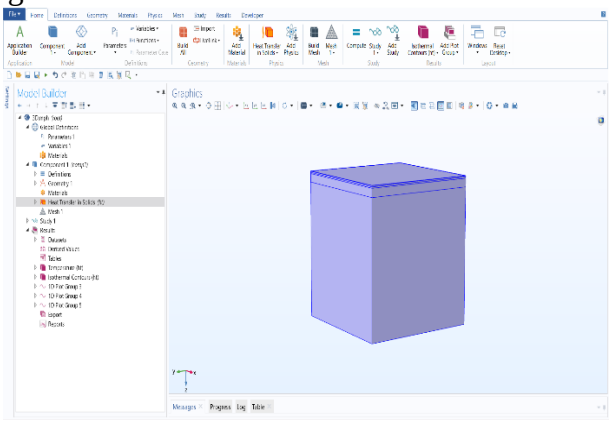

Figure 2. 3-D model interface in COMSOL Multiphysics.

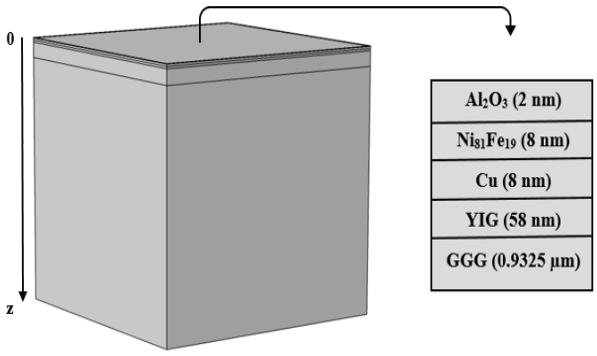

Figure 3. The COMSOL Multiphysics geometry of the sample in a 3-D model, with a schematic showing the thickness of each layer.

The thermal and optical parameters used in the measurements of thermal flow and optical absorption are displayed in Table 1. The material parameters are assumed to be temperature independent and not to change as a result of optical excitation.

Table 1. The thermal and optical parameters for the materials used in the calculation with an ambient temperature of 300K.

Parameter Unit	Al_2O_3	Py	Cu	YIG	GGG
Density kg/m^3	3890	8700	8930	5170	7080
Thermal conductivity W/m/K	1–4.5 [29]	46.4 [30]	150 [31]	6.63 [32]	7.94 [32]
Heat capacity J/kg/K	880	430	385	578	400
Refractive index n (800 nm)	1.759	2.2 + j3.6 [33]	0.24991 + j5.0337	2.19 + j2.48 × 10^{-6} [34]	1.95

The laser pulse is essential in this study since it represents the source of heat falling on the sample. The wavelength of the laser used is 800 nm. The laser spot diameter is 120 µm (Since the diameter

of the laser spot is significantly larger than the thickness of the stack, lateral heat diffusion at the sample's surface can be overlooked). The FWHM laser pulse width (t) is assumed to be 74 fs, while the laser repetition rate (f) is 100 kHz. Therefore, the peak power (P) in mW is as follows:

$$P = \frac{\text{power}\ (mW)}{f \times t} = \text{power}\ (mW) \times 1.3514 \times 10^{8} \quad (7)$$

o account for the imperfect contact between the various layers in the stack, thermal-boundary resistance (TBR) interface conditions were used in the numerical simulations in COMSOL Multiphysics.

An assumed value of TBR = 2×10^{8} W/m^2/K for the Al_2O_3/$Ni_{81}Fe_{19}$ and Cu /YIG interfaces [35, 36], while values of 1×10^{9} and 2.04×10^{8} W/m^2/K were gathered for $Ni_{81}Fe_{19}$ /Cu and YIG/GGG [36], respectively.

RESULTS AND DISCUSSION

The results are based on the measurements of a trilayer thin metallic film (Py/Cu/YIG) heated by an ultrafast laser. A number of investigations have been conducted to observe the temperature change induced by a fs laser within the trilayer sample, which gives a clear visualization of the spin current generated within the sample.

The temperature distribution inside the trilayer sample was observed in Figure 4 (Temperature is represented by the color legend) as a result of optical pumping by an ultrafast fs laser at selected time delays.

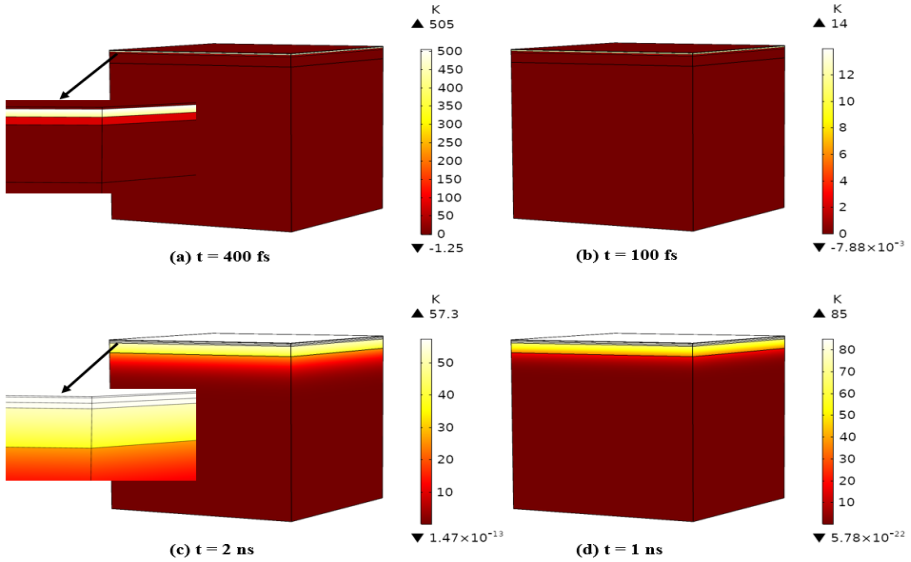

Figure 4. Temperature distribution within the trilayer sample at selected time delays. TBR is included in the calculations.

Figure 5 shows a significant rise in the temperature of the Permalloy layer at the time of 400 fs and then the entire energy absorption at the Cu/YIG interface. At a time of 0.05 ns, a thermal gradient occurs within the sample (YIG) indicating the generation of a spin current. At 100 fs, a small rise in temperature is almost negligible.

The temperature change at different depths inside the sample is shown in Figure 6 (The relationship takes a logarithmic form to simplify and expand the shape) as a function of time with the addition of TBR. At time 400 fs and depth 6 nm, there was a significant rise in Py temperature. Thermal conduction from the metallic overlayers allows the temperature inside the YIG layer to increase on a time scale of around 1 ns. In the Cu/YIG interface, we observe a marked rise in temperature over a time scale of 0.05 ns. The temperature in this interface (Cu/YIG) is important in determining the spin current generated inside the YIG by ultrafast laser.

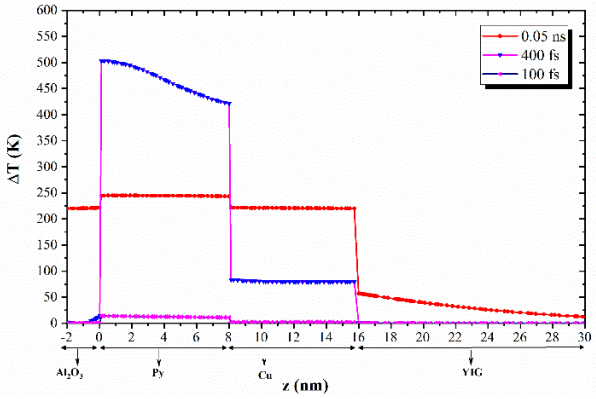

Figure 5. Change in temperature as a function of depth within the trilayer sample at selected time delays. TBR is included in the calculations.

Figure 7 shows the temperature gradient at selected positions within the YIG layer, which is heavily impacted by the sample's position z relative to the surface. The presence of a significant thermal gradient at the Cu/YIG contact emphasizes the need for using TBR in calculations.

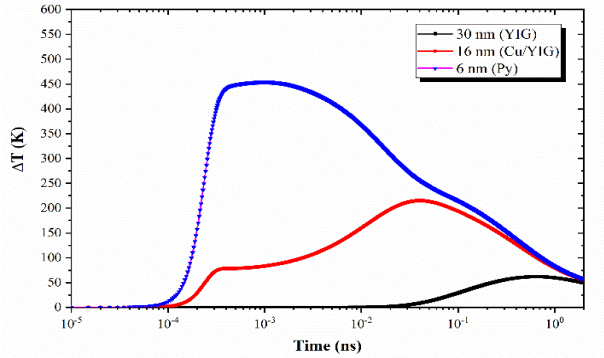

Figure 6. Change of temperature as a function of time at selected depths within the trilayer sample. TBR is included in the calculations.

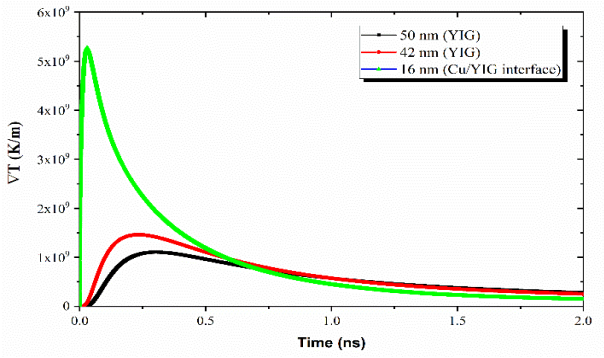

Figure 7. Temperature gradient as a function of time within the trilayer sample. TBR is included in the calculations.

Figure 8 illustrates the temperature change in the YIG layer as a function of Py layer thickness. The temperature differential in the YIG layer increases as the thickness of the Py changes. At 8 nm thickness and 0.05 ns time, the maximum temperature was observed. This can save energy and allow for the use of a low-power laser.

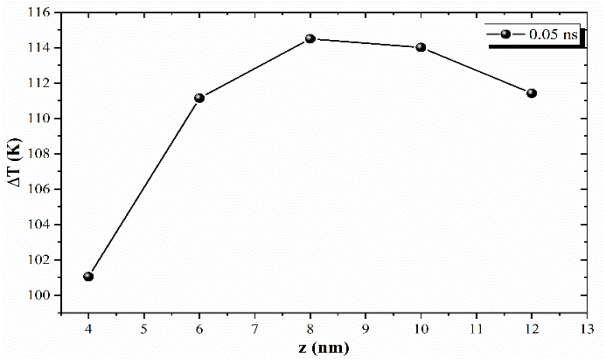

Figure 8. Change of temperature as a function of Py thickness within the YIG layer at a time of 0.05 ns. TBR is included in the calculations.

Conclusion

This study aims to simulate the thermal gradient to generate a pure spin current within the magnetic insulator (YIG) using an ultrafast fs laser in a multilayer thin film. Simulation results showed:

1. The effect of thickness and time on the generation of spin current induced by optical pumping within a trilayer (Py/Cu/YIG).
2. A significant rise in the temperature of the permalloy layer was detected as a result of excitation by a fs laser pulse, followed by energy absorption in the copper layer, which leads to a thermal gradient within the sample (YIG) at times of 0.05 and 1 ns, indicating the generation of spin current.
3. The Cu/YIG interface was discovered to be very important in spin current generation, indicating the importance of including TBR values in calculations.
4. The thickness of the Py layer has been shown to be necessary to generate a high-temperature gradient within the magnetic insulator to generate a spin current where the maximum temperature was observed at 8 nm thickness and 0.05 ns time.

References

[1] F. Bottegoni, C. Zucchetti, F. Ciccacci, M. Finazzi, and G. J. A. P. L. Isella, "Optical generation of pure spin currents at the indirect gap of bulk Si," vol. 110, no. 4, p. 042403, 2017.

[2] D. Wu *et al.*, "Pure spin current generated in thermally driven molecular magnetic junctions: a promising mechanism for thermoelectric conversion," vol. 7, no. 32, pp. 19037-19044, 2019.

[3] Y. Zhou, S. Yu, and X. J. C. Zheng, "Edge passivation control of graphene nanoribbons for robust pure spin current generation with photogalvanic effect," vol. 170, pp. 361-367, 2020.

[4] J. C. J. J. o. M. Slonczewski and M. Materials, "Current-driven excitation of magnetic multilayers," vol. 159, no. 1-2, pp. L1-L7, 1996.

[5] L. J. P. R. B. Berger, "Emission of spin waves by a magnetic multilayer traversed by a current," vol. 54, no. 13, p. 9353, 1996.

[6] S. Valenzuela and M. J. J. o. a. p. Tinkham, "Electrical detection of spin currents: The spin-current induced Hall effect," vol. 101, no. 9, p. 09B103, 2007.

[7] S. Takahashi, S. J. S. Maekawa, and T. o. A. Materials, "Spin current, spin accumulation and spin Hall effect," 2008.

[8] A. J. I. t. o. m. Hoffmann, "Spin Hall effects in metals," vol. 49, no. 10, pp. 5172-5193, 2013.

[9] S. Bhuktare, H. Singh, A. Bose, and A. A. J. P. R. A. Tulapurkar, "Spintronic oscillator based on spin-current feedback using the spin hall effect," vol. 7, no. 1, p. 014022, 2017.

[10] K. Uchida *et al.*, "Observation of the spin Seebeck effect," vol. 455, no. 7214, pp. 778-781, 2008.

[11] H. Adachi, K.-i. Uchida, E. Saitoh, and S. J. R. o. P. i. P. Maekawa, "Theory of the spin Seebeck effect," vol. 76, no. 3, p. 036501, 2013.

[12] R. Ramos *et al.*, "Temperature dependence of the spin Seebeck effect in [Fe3O4/Pt] n multilayers," vol. 7, no. 5, p. 055915, 2017.

[13] Y. Hu, H. Wu, Y. Meng, and D. B. J. J. o. A. P. Bogy, "Nanoscale thermal analysis for heat-assisted magnetic recording," vol. 122, no. 13, p. 134303, 2017.

[14] R. Pitchumani, J. Hughes, and E. L. Miller, "SMRDB: key-value data store for shingled magnetic recording disks," in *Proceedings of the 8th ACM International Systems and Storage Conference*, 2015, pp. 1-11.

[15] T. R. Albrecht *et al.*, "Bit-patterned magnetic recording: Theory, media fabrication, and recording performance," vol. 51, no. 5, pp. 1-42, 2015.

[16] S. Greaves, Y. Kanai, and H. J. I. T. o. M. Muraoka, "Multiple layer microwave-assisted magnetic recording," vol. 53, no. 2, pp. 1-10, 2016.

[17] M. Kief and R. J. M. B. Victora, "Materials for heat-assisted magnetic recording," vol. 43, no. 2, pp. 87-92, 2018.

[18] J.-G. Zhu and H. J. I. t. o. m. Li, "Understanding signal and noise in heat assisted magnetic recording," vol. 49, no. 2, pp. 765-772, 2013.

[19] T. W. J. J. o. A. P. McDaniel, "Application of Landau-Lifshitz-Bloch dynamics to grain switching in heat-assisted magnetic recording," vol. 112, no. 1, p. 013914, 2012.

[20] S. Xiong *et al.*, "Setting write spacing in heat assisted magnetic recording," vol. 54, no. 8, pp. 1-7, 2018.

[21] H. Mohamad *et al.*, "Thermally induced magnetization dynamics of optically excited YIG/Cu/Ni 81 Fe 19 trilayers," vol. 96, no. 13, p. 134431, 2017.

[22] "COMSOL Multiphysics Reference Manual, Version 5.5," 2019.

[23] K. Sugioka, Y. J. L. S. Cheng, and Applications, "Ultrafast lasers—reliable tools for advanced materials processing," vol. 3, no. 4, pp. e149-e149, 2014.

[24] W. Zhao and L. J. P. Wang, "Microdrilling of through-holes in flexible printed circuits using picosecond ultrashort pulse laser," vol. 10, no. 12, p. 1390, 2018.

[25] E. Mottay, X. Liu, H. Zhang, E. Mazur, R. Sanatinia, and W. J. M. b. Pfleging, "Industrial applications of ultrafast laser processing," vol. 41, no. 12, pp. 984-992, 2016.

[26] J.-C. Kieffer, S. Fourmaux, and A. Krol, "The ultrafast high-peak power lasers in future biomedical and medical x-ray imaging," in *19th International Conference and School on Quantum Electronics: Laser Physics and Applications*, 2017, vol. 10226, p. 1022612: International Society for Optics and Photonics.

[27] E. Mirkoohi, D. E. Seivers, H. Garmestani, and S. Y. J. M. Liang, "Heat source modeling in selective laser melting," vol. 12, no. 13, p. 2052, 2019.

[28] A. J. J. Crook, "The reflection and transmission of light by any system of parallel isotropic films," vol. 38, no. 11, pp. 954-964, 1948.

[29] B. Su-Yuan, T. Zhen-An, H. Zheng-Xing, Y. Jun, and W. J. C. P. L. Jia-Qi, "Thermal conductivity measurement of submicron-thick aluminium oxide thin films by a transient thermo-reflectance technique," vol. 25, no. 2, p. 593, 2008.

[30] A. Avery, S. Mason, D. Bassett, D. Wesenberg, and B. J. P. R. B. Zink, "Thermal and electrical conductivity of approximately 100-nm permalloy, Ni, Co, Al, and Cu films and examination of the Wiedemann-Franz Law," vol. 92, no. 21, p. 214410, 2015.

[31] W. Liu, Y. Yang, and M. Asheghi, "Thermal and electrical characterization and modeling of thin copper layers," in *Thermal and Thermomechanical Proceedings 10th Intersociety Conference on Phenomena in Electronics Systems, 2006. ITHERM 2006.*, 2006, pp. 1171-1176: IEEE.

[32] A. M. J. P. Hofmeister and C. o. Minerals, "Thermal diffusivity of garnets at high temperature," vol. 33, no. 1, pp. 45-62, 2006.

[33] G. Neuber *et al.*, "Temperature-dependent spectral generalized magneto-optical ellipsometry," vol. 83, no. 22, pp. 4509-4511, 2003.

[34] T. Goto, M. C. Onbaşlı, and C. J. O. e. Ross, "Magneto-optical properties of cerium substituted yttrium iron garnet films with reduced thermal budget for monolithic photonic integrated circuits," vol. 20, no. 27, pp. 28507-28517, 2012.

[35] B. C. Gundrum, D. G. Cahill, and R. S. J. P. R. B. Averback, "Thermal conductance of metal-metal interfaces," vol. 72, no. 24, p. 245426, 2005.

[36] M. Schreier *et al.*, "Magnon, phonon, and electron temperature profiles and the spin Seebeck effect in magnetic insulator/normal metal hybrid structures," vol. 88, no. 9, p. 094410, 2013.